Lab and Field Scale Modeling of Near Miscible CO_2 Injection in Different Porous Mediums

Mohammad Parvazdavani*, Seyed Mahdia Motahhari, and Vahid Ansari

Reservoir Studies Research Division, Research Institute of Petroleum Industry (RIPI), Tehran, Iran

ABSTRACT

The main purpose of this investigation is to study the effect of near miscible CO_2 injection in different porous mediums on both lab and field scales. This effect can be traced by the change of two-phase gas-oil relative permeability curves. In this work, the experiments have been performed on three rock types (i.e. sandstone, dolomite, and artificial fractured sandstone) based on an incremental pressure algorithm approaching a near miscible condition. Lab-scale inverse modeling has been used to calculate relative permeability curves. Based on the experimental results, 85%of minimum miscibility pressure was defined as the near miscible pressure. Comprising the relative permeability curves in immiscible and near-miscible conditions, the results show that this change has become less significant from sandstone core type to artificial fractured. In other words, near miscible CO_2 injection would be recommended in rock types with a lower RQI. In addition, it was concluded that in the case of artificial fractured, simple conventional relative permeability methods obtain the same results as sophisticated inverse modeling method. Furthermore, in order to validate the lab scale results, the field scale modeling of the candidate reservoir was done using the 3D compositional reservoir simulator. 83% of minimum miscibility pressure was defined as near miscible pressure. Moreover, the simulation results confirmed lab-scale data regarding the recovery factor in different rock types. Additionally, the economic evaluation (NPV analysis) showed that use of near miscible CO_2 injection in lower RQI reservoirs was more economical rather than the other scenarios.

Keywords: Near-miscible CO_2 Injection, Lab and Field Scale, Inverse Modeling, Rock Types, Relative Permeability Curves, NPV Analysis

INTRODUCTION

Recently, carbon dioxide injection has been employed as a secondary or tertiary oil recovery method. Experimental studies showed that oil recovery factor after CO_2 injection improved up to 60% of original oil in place as the tertiary method, while this value was only 44% for water flooding as the secondary method [1].

Dong et al. indicated that miscible CO_2 flooding was unfavorable for some reservoirs in southeast Saskatchewan due to high CO_2 minimum miscibility pressure or some available limitations on providing the required operational pressure. Their results showed that oil recovery was improved during near-miscible CO_2 injection and it could be inferred that the mechanism of oil mobilization in the CO_2 miscible and near-miscible injection was the

***Corresponding author**

Mohammad Parvazdavani

Email: mohammadparvazdavani@yahoo.com

Tel: +98 21 4825 5332

Fax: +98 21 4473 9731

Article history

Received: July 17, 2013

Received in revised form: November 17, 2013

Accepted: January 26, 2014

Available online: February 20, 2015

same [2].

This increase in oil recovery is because of the changes in oil and gas relative permeability. Under miscible conditions, when the interfacial tensions between oil and gas phases decreases, the values of the relative permeability change; it is a function of the phase behavior of working fluids, their physical properties, and porous media characterization [3,4]. Al-Wahaibi et al. studied the two-phase drainage and imbibition relative permeability curves under different equilibrium conditions. They showed that when IFT decreased, the relative permeability curve of non-wetting phase changed more considerably than the wetting phase curve and hysteresis became no significant [3-5].

There are three major approaches toward the determination of two-phase relative permeability from unsteady state displacement experiments: analytical, semi analytical and history matching methods [6].

The possibility of overcoming the defects regarding the analytical and semi analytical methods encourages us to use the history matching method by using the inverse modeling technique to calculate the relative permeability values.

Very few experimental studies have been done to investigate the effect of near miscible CO_2 injection on oil recovery in various ranges of rock types. Trivedi and Babadagli provided an excellent review on practical recipes for CO_2 injection in fractured reservoirs. To make the experts capable of selecting the suitable rock type for applying the economic gas injection approach, an experimental study has been done with various rock types ranged from sandstone to dolomite to an artificial fractured rock from Iranian oil fields, which contains different levels of very low permeable to high permeable porous medias [7].

In this study, in the second section, lab scale experiments have been done to find the near miscible pressure and extract the production data. Then, in the third section, a lab scale inverse modeling has been performed to determine the relative permeability curves. By the analysis of the relative permeability curves, we aimed to determine the effect of near miscibility injection as an EOR method in different rock types. In the fourth section, a sector field scale modeling has been conducted to testify the accuracy of the lab test results. In the fifth section, an NPV analysis has been carried out to investigate the economical possibility of near miscible injection in different rock types. Finally, in the sixth section, the results have been discussed on both lab and field scales.

Lab-scale Experiments

Materials

A light oil sample is prepared from one of the west Iranian oil reservoirs and carbon dioxide as the injection gas is almost pure. The physical properties of oil and the lumped heavy component under the standard condition are shown in Table 1. The oil composition shown in Table 2 was determined by gas chromatography (GC) analysis [8].

Table 1: Fluid physical properties

Parameter (at 14.7 psi and 60 °F)	Value
API	41
Viscosity (μ_o) (cP)	3.25
Molecular Weigh (g/mol)	93.18
Density (ρ_l) (g/cc)	0.82
C_{12+} molecular weight (g/mole)	250
C_{12+} density (g/cc)	0.86
CO_2 Viscosity (μ_g) (cP)	0.014473
CO_2 density (ρ_v) (g/cc)	0.0018687

Table 2: Distribution of lab used oil components

Component	Molar percentage(%)
H_2S	0.88
CO_2	0.9
C_1	34.45
C_2	8.37
C_3	5.45
IC_4	1.66
NC_4	3
IC_5	1.92
NC_5	1.93
FC_6	3.05
FC_7	3.23
FC_8	4.16
FC_9	4.62
FC_{10}	2.38
FC_{11}	2.33
C_{12+}	21.67

MMP Determination

Slim-tube experiment was simulated using a 3D compositional simulator with the tuned Peng Robinsun (PR) EOS. The simulator was run and the ultimate oil recovery was calculated after 1.2 hydrocarbon pore volume (HCPV) in various incremental pressure steps. The plot of oil recovery versus pressure is shown in Figure 1. Minimum contact miscibility (MCM) pressure has been defined 950 psia as the refraction point (Figure 1). To investigate the pressure, the gas injection process was simulated by commercial software and total recovery factor at different stages of injection pressures were calculated. The pressure, at which the slope of the increase in the recovery factor was the highest and leveled off to zero afterwards, was called the near miscible pressure (85% of MMP (i.e. 800 psia)) (Figure 2). Thus 500 psia has been defined as the immiscible pressure and 800 psia is considered as the near miscible pressure [9, 10].

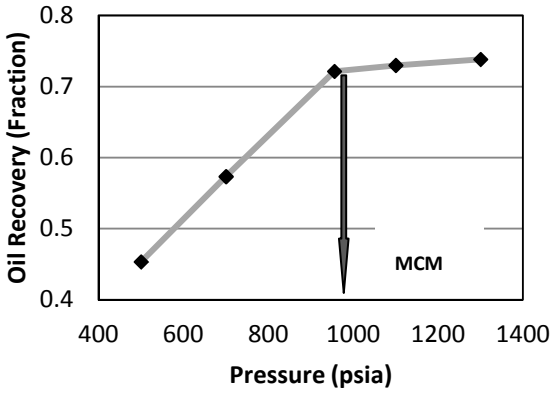

Figure 1: Oil recovery versus pressure in slim-tube simulation

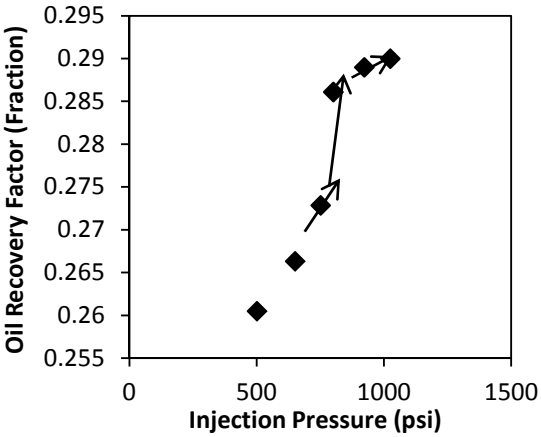

Figure 2: Oil recovery versus pressure in simulated gas injection through sandstone on lab scale

Core Properties

The displacement tests were performed on the low permeable (low reservoir quality index (RQI)) sand stone core sample and dolomite one (moderate RQI) from the south part of Iranian oil fields and their detailed information is shown in Table 3. To prepare the rock type with a high RQI value and investigate the effect of near miscibility on artificial fractured core types, fracturing process has been done on the sandstone core type. By this process, the obtained core had an absolute permeability of 459.3 mD, but its porosity was in range of the sandstone core sample.

Table 3: Sandstone/dolomite core sample Properties

Parameters		Dolomite	Sandstone
Length (L)	cm	5.37	6.59
Area(A)	cm^2	11.35	10. 95
Pore volume (PV)	cm^3	8.45	9.47
Porosity(φ)	Fraction	0.1386	0.1313
Permeability (K)	mD	16.45	1.31

Apparatus and Experimental Procedure

In this experimental work, the unsteady state displacement technique was used; the schematic diagram of relative permeability measurement apparatus is shown in Figure 3. By measuring the volume of oil and gas, and the corresponding pressure drop, the production data will be recorded dynamically. The relative permeability values have been calculated by analyzing the production data.

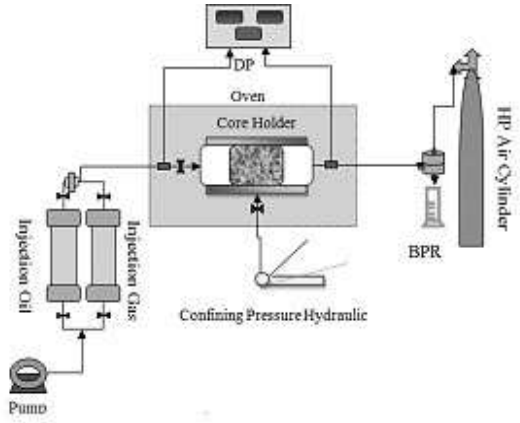

Figure 3: Plan of the experimental setup

First, the core is solvent cleaned, dried with hot nitrogen, and evacuated. After core preparation, the core was saturated by the saturator apparatus with the brine solution (10000 ppm). After the operational preparation (Table 4), absolute permeability was calculated by monophonic core flood test. Then, oil was injected into the core at the rate of 0.05 (cm^3/min) to reach irreducible water. Next, gas was injected at the rate of 0.05 (cm^3/min) up to 2 PV. The amount of the produced oil and gas was measured by camera tracker dynamically. The tests were done according to pressure steps from immiscible to near miscible condition and implemented by BPR.

Table 4: Core flooding set values

Parameter		Value
(pressure of back pressure regulator) BPR_P	psia	Two points 500 and 800
Overburden pressure	psia	BPR_P+650
Time interval for data recording	sec	10

Lab-scale Inverse Modeling

Inverse modeling (i.e. history matching technique) has been used to extract the relative permeability curves implicitly. In this approach, JBN method (1959) was firstly used to calculate the relative permeability as an initial guess, where it was used in compositional fluid flow simulation. Then, the production data from the simulator were compared with the experimental results. Finally, the difference between the experimental production results and simulation data was minimized by using a suitable optimization algorithm (classical conjugate gradient approach). The results of relative permeability obtained from the last step of the optimization process were defined as the implicit values [11].

JBN method extracts relative permeability curves individually based on Equation 1. The terms of W_i and I_r are determined through Equations 2 and 3 [11].

$$\frac{d(\frac{1}{W_i\, I_r})}{d(\frac{1}{W_i})} = \frac{f_o}{Kr_o} \quad (1)$$

$$W_i = \frac{1}{f'} = \frac{1}{\frac{df}{ds}} \quad (2)$$

$$I_r = \frac{\frac{u}{\Delta P}}{\frac{u_s}{\Delta P}} \quad (3)$$

$$Kr_g = \frac{1 - f_o}{f_o} \frac{\mu_g}{\mu_o} Kr_o \quad (4)$$

Relative permeability curves are drawn based on outlet gas saturation (Equation 5) and the value of $S_{g\,(ave)}$ in Equation 5 can be obtained by mass balance.

$$S_{g\,(2)} = S_{g\,(ave)} - W_i\,(f_o)_2 \quad (5)$$

In the second part (i.e. one dimensional, two-phase compositional simulation), where the values of initial relative permeabilities were embedded, the static model of simulator is firstly built in one dimensional (i.e. 11 grids in z-direction and 1 grid in the other two directions) based on the petro-physical data of core sample (Figure 4). Then, the dynamic behavior of fluid flow (i.e. gas injection process) is simulated fully implicit. The production results extracted from the simulation are history matched with the experimental results by using an optimizing process (conjugate gradient method) [12]. In this optimization process, the independent variable (*x*) is equivalent to K_r as the controlling parameter, and the objective function (*F*) is equivalent to the absolute difference of the production result (i.e. q_0 as the cumulative oil production) obtained by both experiments and simulation. By minimizing the objective function, the ultimate values of relative permeability were considered as the implicit values.

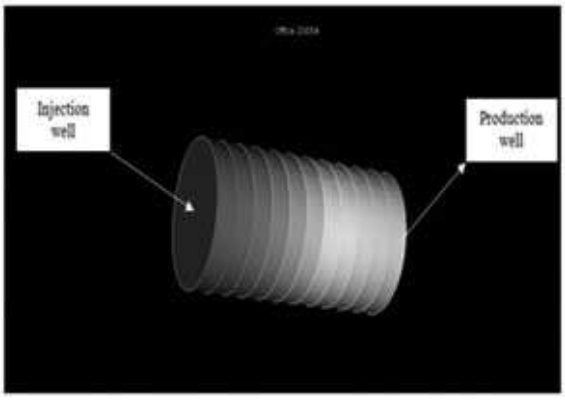

Figure 4: A schematic of core sample developed by the static model of compositional simulator

Field-scale Modeling

To investigate the near miscibility effect and to testify the obtained lab-scale results on field scale, a sector model has been constructed from the candidate reservoir. The sampled sector has eight injectors and one producer (Figure 5).

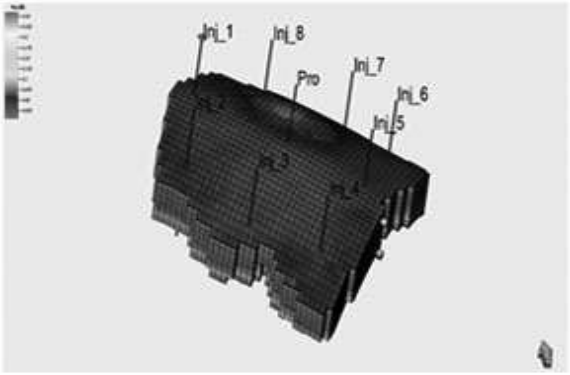

Figure 5: Constructed sector model

The total rock and fluid properties of the sector model have been shown in Table 5, 6, and 7. To use the miscible CO_2 injection on field scale, the screening criteria of this method has been analyzed based on the reservoir characteristics (Table 8).

Table 5: Properties of constructed sector model

Phi	**0.01**	**0.26**	**0.19**
PermX	0.01	214.14	56.67
PermY	0.01	214.14	56.67
PermZ	0.00	189.13	40.42

By running the slim-tube experiment using compositional simulation, multiple contact miscible pressure, 3100 psi, has been defined for the case of CO_2 injection into candidate reservoir fluid at reservoir temperature (T=260 °F). Different development strategies have been defined for the generation of successive increasing pressure algorithms as well as the laboratory set pressures. By running the strategies in case of candidate reservoir defined as lower RQI, (see the total information of strategies in Table 9), the pressure at which the oil saturation around the wellbore region of injection wells started to become less than the residual oil saturation would be called

near miscible pressure. At this pressure, the IFT values between the injected gas and reservoir oil started to decrease and vaporizing mechanisms have been activated. To trace this pressure, like the laboratory phase, the recovery factor for each injection step has been plotted versus its injection pressure.

Table 6: Distribution of field used oil components

Parameter	Min	Max	Mean
Component	Residual Oil (mole %)	Associated Gas (mole %)	Reservoir Oil (mole %)
H_2S	0.00	0.00	0.00
N_2	0.00	0.83	0.36
CO_2	0.00	1.17	0.51
C_1	0.00	57.69	25.24
C_2	0.08	17.98	7.91
C_3	1.10	11.11	5.48
IC_4	0.59	1.70	1.07
NC_4	2.38	4.68	3.39
IC_5	1.52	1.31	1.42
NC_5	1.92	1.48	1.73
C_6	7.81	1.33	4.98
C_7^+	4.20	0.54	2.60
Molecular Weight of Residual Oil			243.0000
Molecular Weight of C_{12}^+ Fraction			325.0000
Molecular Weight of Reservoir Oil			149.0000
Sp. Gr. of C_{12}^+ Fraction (60/60 °F)			0.9567

Table 7: Fluid properties of field used oil

Parameter		Value
Bubble Point Pressure	Psia	1730
Solution Gas Oil Ratio	SCF/STB	430
Producing Gas Oil Ratio	SCF/STB	325.6
Oil FVF	bbl/STB	1.2398
Initial Reservoir Pressure	psia	1900
Oil Viscosity	cP	0.9520

The inflection point, 2600 psia, has been reported as the near miscible pressure (Figure 6). Then, the strategies have been repeated for the case of higher RQI (with higher permeability anisotropy and value) to trace the effect of near miscibility on the artificial fractured rock type on field scale.

Table 8: Screening criteria for CO_2 injection

Parameter		Value
Gravity	API	22-45 (Ave: 37)
Viscosity	cP	0-35 (Ave: 2.1)
Porosity	%	3-35 (Ave: 14.8)
Oil saturation	% (PV)	15-89 (Ave: 46)
Formation Type	-	Sandstone/Carbonate
Permeability	mD	1.5-4500 (Ave: 201.1)
Net thickness	ft	Wide range
Depth	ft	1500-13365 (Ave: 6171.2)
Temperature	°F	82-260 (Ave: 136.3)

Table 9: Total information on used strategies on field scale modeling

Parameter		Value
Minimum Bottom Hole Pressure for Production well	psia	1800
Maximum Bottom Hole Pressure for Injection well	psia	2100, 2600, 3100
Minimum GOR for Production well	SCF/STB	1.5
Production Time Interval	Years	40

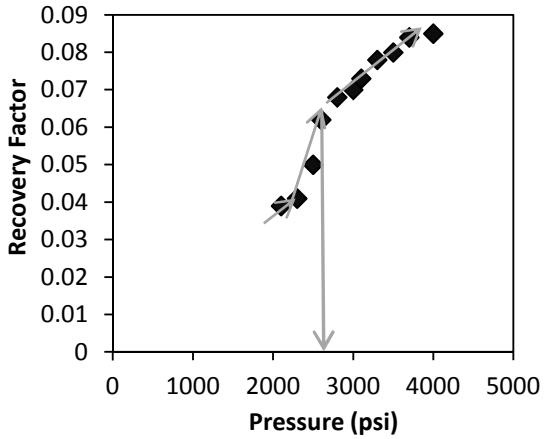

Figure 6: Oil recovery versus pressure in simulated gas injection into the reservoir on field scale

Economical Evaluation

To investigate the economical possibility of near miscible injection compared to the other ones, net present values (NPV) analysis has been done

for three scenarios: miscible injection, 3100 psia; near miscible, 2600 psia; and immiscible, 2100 psia.

Since CO_2 has a low liquefied pressure at the reservoir temperature compared to other injection gases, two successive steps, namely compressor and pump, are necessary to increase the pressure. In each step, power calculation has first been performed to find the required power for the delivery of CO_2 into reservoir at the desired injection pressure. In the second step, capital and operational costs including the electrical power have been calculated. Finally, net present value has been calculated for each pressure.

To calculate the required power, the initial and final pressures of compressors have been defined 14.7 psia and 1085 psia (liquefied pressure at ambient temperature) respectively. Pumps transfer the flow from the final pressure of the compressor to set pressure in each scenario.

Compressor Power Calculations

The compression power requirement for each stage ($W_{s,i}$) is given by Equation 6 [13, 14].

$$W_{s,i} = \left(\frac{1000}{24 \times 3600}\right) \left(m \times \frac{Z_s R T_{in}}{M \eta\, is}\right) \left(\frac{k_S}{k_S - 1}\right) \left[(CR)^{k_S - \frac{1}{k_S}} - 1\right] \quad (6)$$

where, for all stages:

R=8.314 kJ/kmol.K

M=44.01 kg/kmol

T_{in}= 313.15 K (i.e., 40 °C)

η_{is} = 0.75

CR is the compression ratio for each stage and calculated by Equation 7.

$$CR = \left(\frac{P_{cut-off}}{P_{initial}}\right)^{\frac{1}{N_{stage}}} \quad (7)$$

where, N_{stage}=5

Values of each parameter for the calculation of compressor power are shown in Table 10 for all the stages. Finally, the total power requirement for the compressor has been defined by Equation 8.

$$W_{s-total} = (W_s)_1 + (W_s)_2 + (W_s)_3 + (W_s)_4 + (W_s)_5 \quad (8)$$

Table 10: Vital values for compressor power calculations

Stage No.	Z_s	K_s	Valid Pressure Range (MPa)	Valid Maximum Temperature (K)
1	0.995	1.277	0.1-0.24	356
2	0.985	1.286	0.24-0.56	356
3	0.970	1.309	0.56-1.32	356
4	0.935	1.379	1.32-3.12	356
5	0.845	1.704	3.12-7.38	356

Pump Power Calculations

The required power can be estimated by Equation 9.

$$W_p = \left(1000 \times \frac{10}{24 \times 36}\right) \times \left[\frac{m\left(P_{final} - P_{cut-off}\right)}{\rho \eta_p}\right] \quad (9)$$

where, m is the CO_2 mass flow rate (tones/day), ρ=630 kg/m^3, and η_p=0.75.

As an example, power calculations of near miscible condition are shown in Figure 7.

Capital Cost Calculations

Capital costs of compressor and pump have been defined by Equations 10 to 13.

$$m_{train} = \frac{(100 \times m)}{(24 \times 3600 \times N_{train})} \quad (10)$$

$$C_{comp} = m_{train} \times N_{train} \left[\begin{array}{l}(0.13 \times 10^6)(m_{train})^{-0.71} + \\ (1.40 \times 10^6)(m_{train})^{-0.6} \ln\left(\frac{P_{Cut-off}}{P_{initial}}\right)\end{array}\right] \quad (11)$$

$$C_{pump} = \left\{(1.11 \times 10^6) \times \left(\frac{W_p}{1000}\right)\right\} + 0.07 \times 10^6 \quad (12)$$

$$C_{total} = C_{comp} + C_{pump} \quad (13)$$

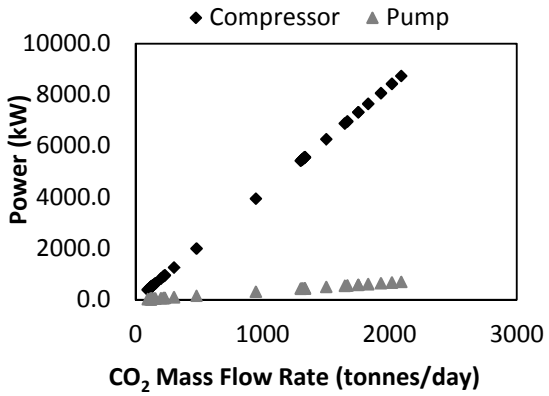

Figure 7: Sampled power calculations for compressor and pump in near miscible condition

The capital cost can be annualized by applying capital recovery factor (CRF) of 0.15.

$$C_{annual} = C_{total} \times CRF \quad (\text{where CF=0.80}) \quad (14)$$

The total amount of CO_2 that must be compressed every year is found by applying a capacity factor (CF) of 0.80.

$$m_{year} = m \times 365 \times CF \quad (\text{where CF=0.80}) \quad (15)$$

The levelized capital costs (C_{lev}) can be defined by Equation 16.

$$C_{lev} = \frac{C_{annual}}{m_{year}} \quad (16)$$

Operational and Maintenance Costs Calculations (O&M)

Annual O&M can be found by applying an O&M factor of 0.04 to the total capital cost.

$$O\&M_{annual} = C_{total} \times O\&M_{factor} \quad (\text{where } O\&M_{factor} = 0.04) \quad (17)$$

The levelized O&M costs ($O\&M_{lev}$) can be defined by Equation 18.

$$O\&M_{lev} = \frac{O\&M_{annual}}{m_{year}} \quad (18)$$

Total Electric Power Costs of the Compressor (E_{comp}) and Pump (E_{pump})

This factor is calculated by multiplying the total power requirement by the capacity factor (CF) of 0.08 and price of electricity (P_c). It can be assumed that the electricity price is 0.065 $ per kWh [15].

$$E_{annual} = E_{comp} + E_{pump} = p_c \times (W_{s\text{-}total} + W_p) \times (CF \times 24 \times 365) \quad (19)$$

The levelized power costs (E_{lev}) can be defined by Equation 20.

$$E_{lev} = \frac{E_{annual}}{m_{year}} \quad (20)$$

Finally, the total annual and levelized costs of CO_2 for compression and pumping have been calculated by Equation 21.

$$\begin{aligned} &Total\ Annual\ Cost\ [\$/yr] = C_{annual} + O\&M_{annual} + E_{annual} \\ &Total\ Levelized\ Cost\ [\$/tonne\ CO_2] = C_{lEV} + O\&M_{lev} + E_{lev} \end{aligned} \quad (21)$$

The last cost item is the price of consumed CO_2, which can be defined based on 5000 $ per 1 MMscf of injection CO_2.

As an example, all of the levelized costs including the total levelized costs for near miscible condition are shown in Figure 8.

RESULTS AND DISCUSSIONS

Six unsteady state displacement experiments have been performed and their production data in the drainage process are used to extract the relative permeability curves using an inverse modeling method. These experiments were carried out at an injection pressure of 500 psi as the immiscible condition and at 800 psi as the near miscible condition for three rock types of core samples with different RQI (sandstone (the lowest RQI), dolomite (moderate RQI), and

artificial fractured sandstone (the highest RQI)). In addition, the length of the core in this study is not enough to establish the situation for near miscibility state. To cover this drawback, the soaking time is considered between the injected gas and crude oil before the effluent fluids are collected. This process facilitates the approach to near miscible condition during the experiments as Asghari and Torabi reported [16].

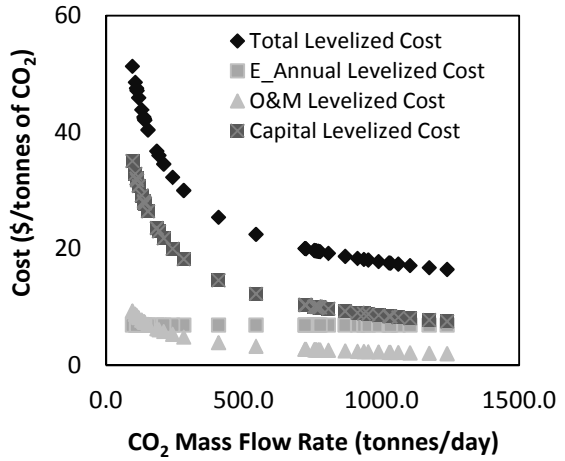

Figure 8: Levelized costs calculations in near miscible condition

To be certain that the near miscible condition was achieved, BSTEN keyword was used on lab scale compositional simulator data file to plot the trend of IFT values around the injection well (Figure 9). This figure shows the decreasing trend of IFT dimensionless value up to 50% of the initial amount as the injection time increased.

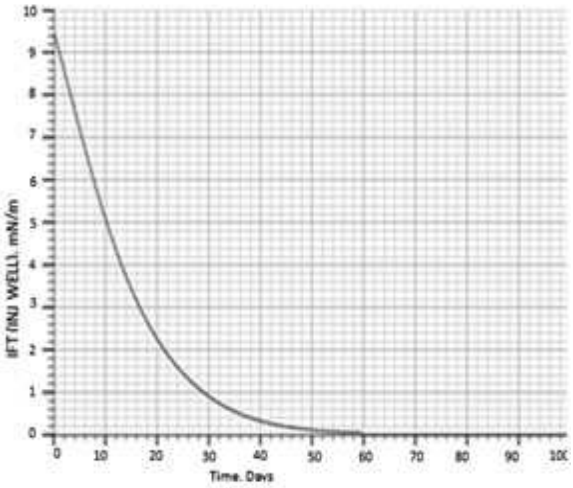

Figure 9: Trend of the change of IFT around the injection well based on elapsed injection time

After the achievement of near miscible condition, the direct production results including cumulative oil production and pressure drop along the core samples were measured (see Figures 10.a and 10.b for sandstone); then, implicit relative permeability curves were extracted (Figures 11, 12, and 13) by using the lab scale inverse modeling method. Finally, on the basis of the relative permeability curves, the effect of near miscibility on the obtained curves was investigated.

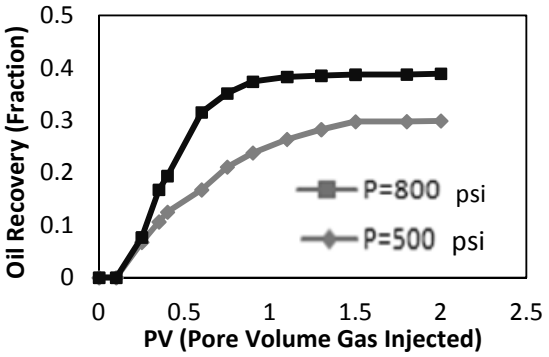

Figure 10.a: Oil recovery comparison in both immiscible and near miscible conditions for sandstone sample

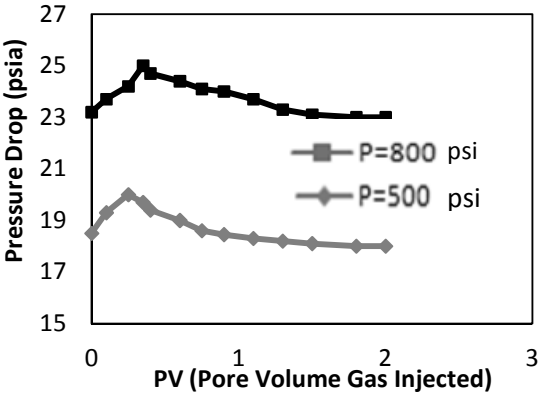

Figure 10.b: Pressure drop comparison in both immiscible and near miscible conditions for sandstone sample

To compare the results of implicit relative permeability curves in cases of immiscible and miscible conditions, the relative permeability curves were plotted based on normalized gas saturation (*Sg* (norm)), which was calculated by Equation 22.

$$S_{g(norm)} = \frac{S_g - S_{g(\min)}}{S_{g(\max)} - S_{g(\min)}} \quad (22)$$

where, $S_{g(\min)}$ and $S_{g(\max)}$ refer to the minimum and maximum outlet gas saturation respectively.

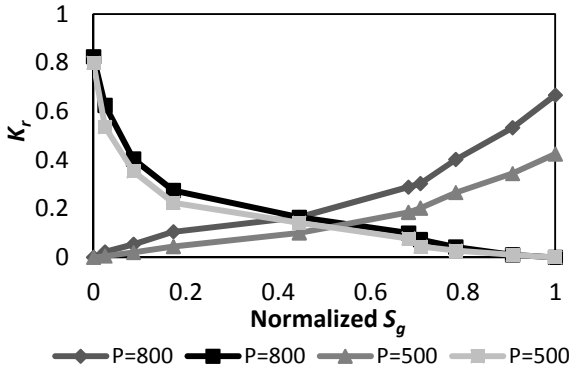

Figure 11: K_r comparison in both immiscible and near miscible conditions for sandstone sample

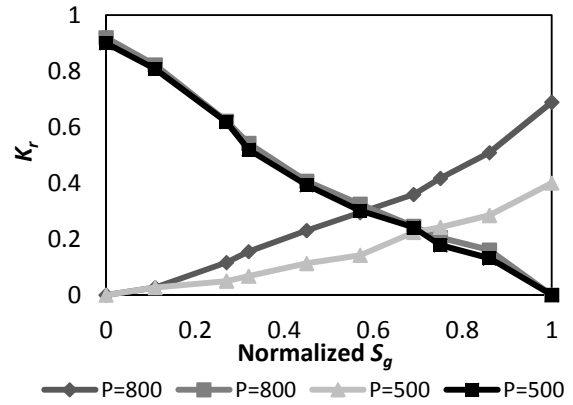

Figure 12: *Kr* comparison in both immiscible and near miscible conditions for dolomite sample

As it can be observed, the change of relative permeability is more dominant for non-wetting gas phase, when the near miscible condition approaches [5]. The main reason is the decrease in oil saturation along the core in the near miscible condition compared to immiscible. This decrease causes more space for gas to pass through itself, which leads to an increase in non-wetting relative permeability curve.

On the other hand, the resistance between oil and gas phases decreases and this change affects the relative permeability of the phase occupied the larger pores (i.e. the non-wetting phase). When there is a high absolute permeability ratio of artificial fractured sample to sandstone sample (K_f/K_s), the gas phase is not tended to pass the matrix part and it passes through fractures. This phenomenon not only causes a decrease in ultimate oil recovery, but also it stabilizes oil saturation along the core in both immiscible and near miscible conditions. This unchanging saturation profile is the reflective of no substantial change of relative permeability curves as shown in Figure 13. In this experiment, this ratio (K_f/K_s) is nearly more than 350 and it can be inferred that, in artificial fractured core samples with a high ratio (K_f/K_s), the effect of near miscibility on changing relative permeability curves is ignorable and the conventional relative permeability methods such as JBN show the same results compared to the sophisticated inverse modeling method (Figure 14).

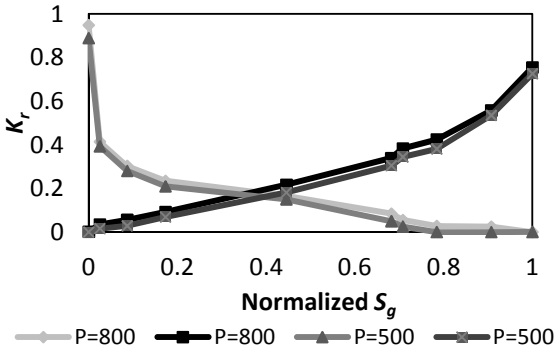

Figure 13: K_r comparison in both immiscible and near miscible conditions for artificial fractured sample

Due to lack of the activation of near miscible mechanisms and successively lack of decrease in ultimate oil saturation (S_{or}), this effect has become less important and not been observed in cases of dolomite and artificial core types respectively (Figures 12 and 13) compared to sandstone result (Figure 11).

This effect on the change of relative permeability curves has been computed by

Equation 23. To have a correlation for this change based on RQI, parameter *E*, calculated by Equation 23, has been plotted versus RQI (Equation 24) as can be seen in Figure 15.

$$E(Error) = \frac{K_{r(o,g)imp} - K_{r(o,g)JBN}}{K\_r(o,g)imp} \quad (23)$$

$$RQI = \sqrt{\frac{K}{\emptyset}} \quad (24)$$

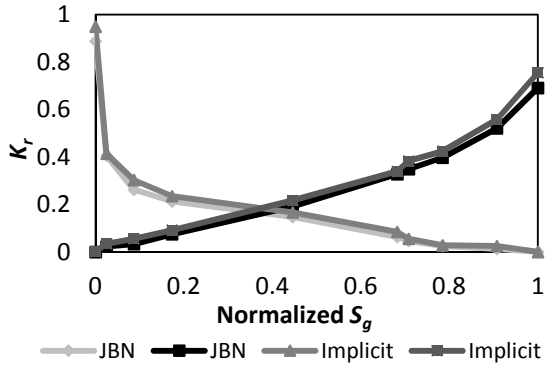

Figure 14: *Kr* comparison in both JBN and implicit inverse modeling method for artificial fractured sample at near miscible condition

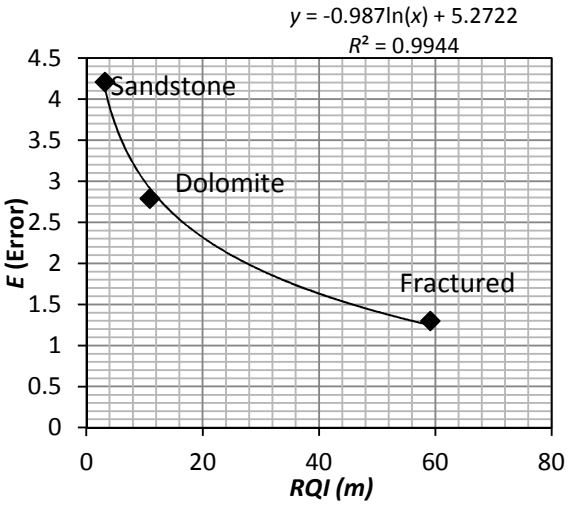

Figure 15: Change of relative permeability values (*E*) versus RQI

To validate the lab scale results, field scale modeling has been investigated using a constructed sector model. The obtained results considers two main issues; it firstly takes into account comprising the daily and cumulative injection and production results in cases of immiscible, near miscible, and miscible conditions as well as economic evaluations for rock types with lower RQI. Secondly, the same procedures have been applied in case of higher RQI (higher *x*-direction permeability leading to more anisotropic reservoir) to investigate the both economic and technical effectiveness of near miscible condition in various rock types on field scale.

The pressures of 2100, 2600, and 3100 psia have been defined as the immiscible, near miscible, and miscible conditions as well as laboratory set pressures. The cumulative oil production was increased by approaching the miscible condition in case of lower RQI reservoirs (Figure 16). The increase of the slope of recovery factor decreased after the near miscible pressure. This trend can be traced from the daily production profile too (Figure 17).

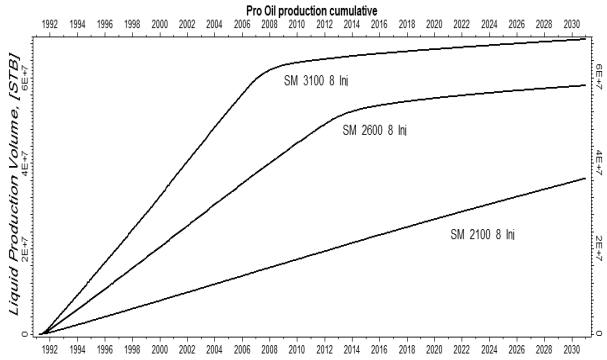

Figure 16: Comparison of cumulative oil production in immiscible, near miscible, and miscible conditions in lower RQI

This phenomenon has happened due to the production of by-passed oil remained in the process of immiscible gas injection. This volume was produced mainly based on the activation of vaporizing mechanism and successively IFT reduction. In this condition, the reduction of IFT between oil and gas phases moved by-passed oil from pore throats to the main oil stream. This condition can be traced by shifting the non-wetting phase saturation into lower value and decrease the curvature of relative permeability in lab scale results, too (Figures 11).

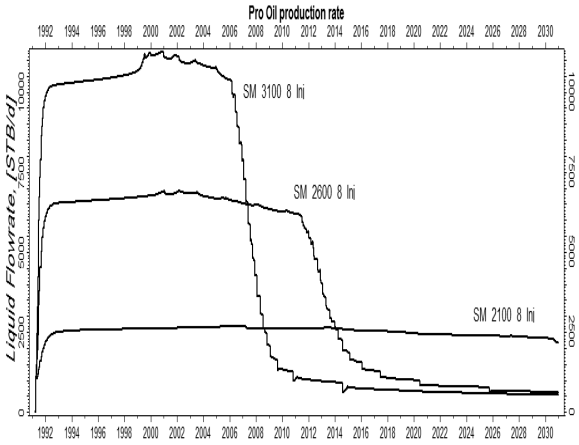

Figure 17: Comparison of oil production rate in immiscible, near miscible, and miscible conditions in lower RQI

To investigate the activation of near miscible mechanisms such as vaporizing in field scale modeling, the oil saturation profile are shown in cases near miscible and miscible injections (Figure 18.a and 18.b). As it can be observed, the oil saturation has been started to decrease to a lesser extent than the residual oil saturation value (0.46) when approaching the miscible condition, which indicates the start of IFT reduction and the activation of near miscibility condition. The corresponding oil saturation values of near miscible and miscible conditions are tabulated in Table 11.

Table 11: Oil saturation profile of specified grid cell in near miscible and miscible conditions in case of lower RQI

Injection Condition	Oil saturation (Fraction)
Near miscible	0.32
Miscible	0.064

To investigate the near miscibility behavior in case of high RQI reservoirs on field scale, a sector with higher *x*-direction permeability (10 times higher) has been constructed to generate the desired anisotropy. The final oil recovery factor was increased by approaching the near miscible condition; however, this increasing ratio, 1.04, was smaller in case of higher RQI than the case of lower RQI, i.e.1.6 (Figure 19).

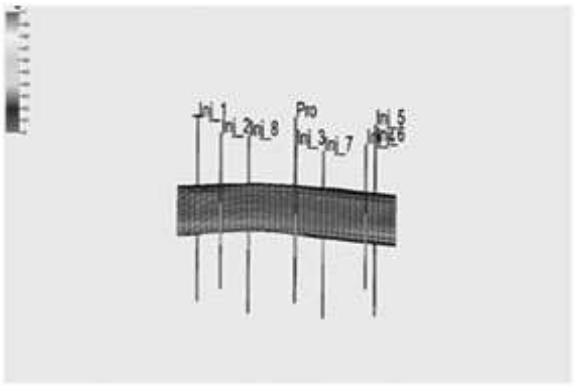

Figure 18.a: Oil saturation profile of the sector model in near miscible condition (P=2600 psia)

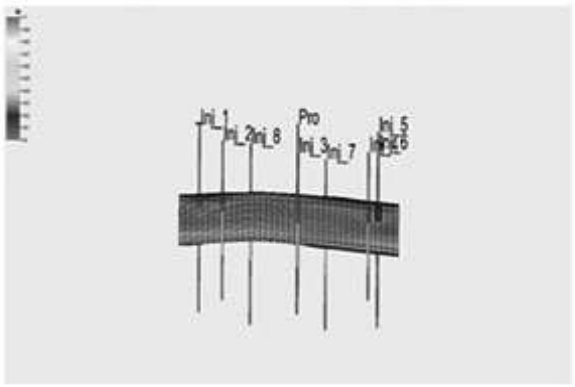

Figure 18.b: Oil saturation profile of sector model in miscible condition (P=3100 psia)

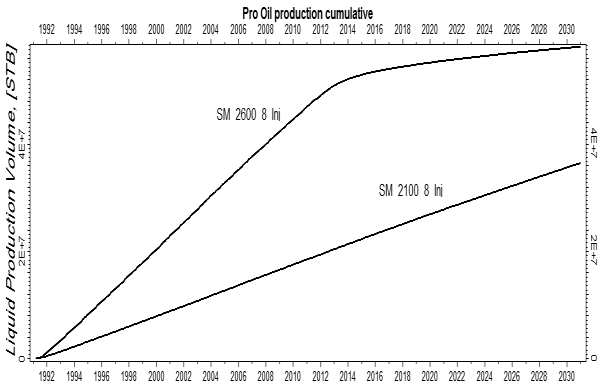

Figure 19: Comparison of cumulative oil production in immiscible and near miscible conditions in higher RQI

In the case of higher RQI reservoirs, oil production did not increase much in near miscible condition compared to the immiscible one. The main reason was due to early breakthrough time and inadequate time for the activation of vaporizing mechanism. This mechanism caused the low rate of mass transfer between two phases. The main

vessel contributed to oil production was fractures or high permeable conduit and very lower volumes were produced through the matrix/low permeable section (i.e. the fracture/conduit storage capacity was high). This phenomenon was recognized as mono-perm-dual porosity model which means the effective permeability of fractures/conduits was the dominant factor in simulation. This dominant model in the oil production of artificial fractured core samples was schematically shown in Figure 20.a. In the case of lower RQI reservoirs, as the gas did not breakthrough earlier, the rate of exchange between two phases of oil and gas were high and the oil was produced through the whole of pore throats (Figure 20.b). Another indicator for earlier breakthrough time was the result obtained on lab scale, i.e. the sharp peak points observed in Figure 21, which happens in lower amount of the PV of the injection gas in case of artificial fractured sample.

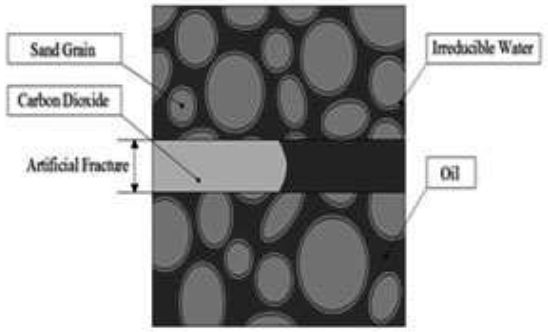

Figure 20.a: A schematic diagram of oil production model in an artificial fractured core type

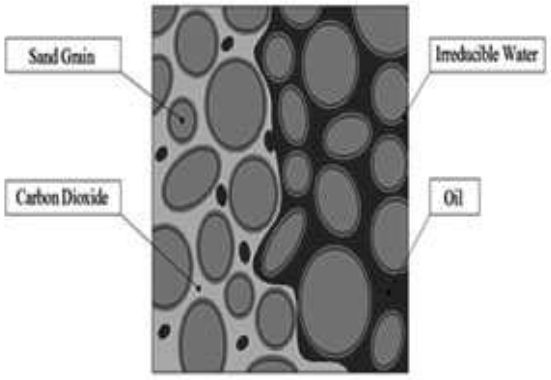

Figure 20.b: A schematic diagram of oil production model in non-fractured core type

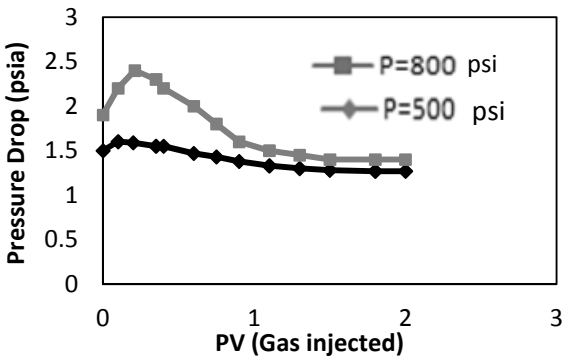

Figure 21: Pressure drop comparison in both immiscible and near miscible conditions for dolomite sample on lab scale

To investigate the economical possibility of near miscible injection compared to the other conditions, NPV analysis has been performed in case of lower RQI (Table 12). To have a better analysis, NPV values have been plotted versus injection pressures in case of lower RQI (Figure 22). As it can be observed, the slope of the increase of NPV decreased and this means that use of near miscible injection is the most economical scenario in case of lower RQI reservoirs. On the other hand, this trend can be traced by the NPV ratio values, which are the ratio of the NPV of each injection stage to the previous one (Table 12). This trend showed a decrease in the ratio, which means gas injection at higher pressures does not increase NPV at the same speed compared to pressures lower than the near miscible pressure.

Table 12: NPV analysis results in case of lower RQI

Pressure (Psia)	Total Cost ($)	Total Income ($)	NPV	NVP ratio
2100	9.869E+07	9.214E+08	8.227E+08	2.354E+00
2600	1.411E+08	2.078E+09	1.937E+09	1.413E+00
3100	1.616E+08	2.899E+09	2.737E+09	1.144E+00
3400	1.537E+08	3.284E+09	3.131E+09	1.111E+00
3700	1.607E+08	3.639E+09	3.479E+09	1.090E+00
4000	1.675E+08	3.958E+09	3.791E+09	1.000E+00

Moreover, NPV and recovery factor values were plotted simultaneously to define the near miscible pressure more certainly. As it can be

observed, the value pointed by the cursor was near miscible pressure at which both NPV and RF curves started to bend and their slopes decreased (Figure 23).

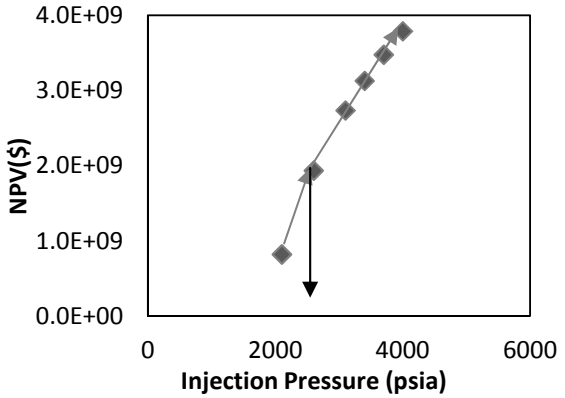

Figure 22: NPV analysis results for injection stages including immiscible, near miscible, and miscible conditions in lower RQI

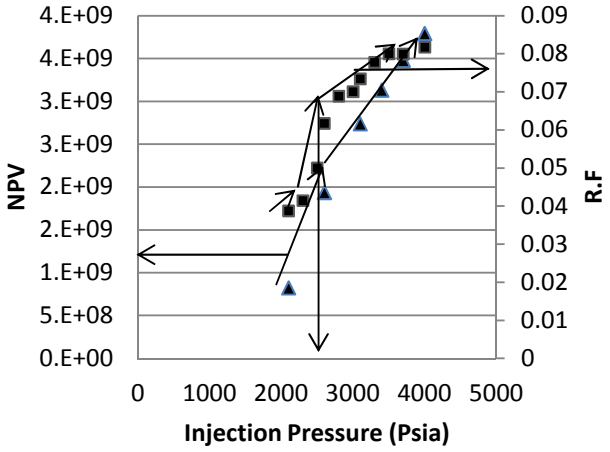

Figure 23: Simultaneous NPV and RF results for injection stages including immiscible, near miscible, and miscible conditions in lower RQI

CONCLUSIONS

To observe the effect of near miscibility on lab scale in different rock types (artificial fractured core, dolomite, and sandstone samples), relative permeability curves have been extracted by lab scale inverse modeling and the results were testified by field sector modeling. The following conclusions can be drawn based on the experiments and modeling results:

- 85% of MMP, obtained by the slim-tube experimental simulation, was reported as the near miscible pressure on lab scale and defined as the inflection point of the curve;
- The effect of near miscibility on two-phase oil-gas relative permeability curves was more significant, moderate, and ignorable in rock types with lower, moderate, and higher RQI respectively;
- In case of artificial fractured core type (higher RQI), the conventional relative permeability methods such as JBN had the same results compared to the sophisticated inverse modeling method;
- Field sector modeling results satisfied lab data regarding the recovery factor in different rock types. 83% of MMP was reported as the near miscible pressure at which mechanisms such as vaporizing activated and oil recovery factor of near miscible injection was near immiscible one in case of higher RQI reservoirs;
- Use of near miscible gas injection in lower RQI reservoirs is more economical rather than the other scenarios.

ACKNOWLEDGMENTS

Authors would like to thank Mr. Safari and Habibi for their useful experience shared.

NOMENCLATURES

f, s	Fracture, sandstone
s	Start of injection
I_r	Injection capacity
	Viscosity
Ø	Porosity
K	Absolute permeability
BPR_P	Pressure of Back Pressure Regulator

Z_s	average CO_2 compressibility for each individual stage [-]
M	Molecular weight of CO_2 [kg/kmol]
K_s	(C_p/C_v) = average ratio of specific heats of CO_2 for each individual stage [-]
m_{train}	CO_2 mass flow rate through each compressor train [kg/s]
1,2	Inlet, outlet of the core
o, g	Oil, gas phase
W_i	Cumulative injection
f	Fractional flow
L	Core length [cm]
A	Cross section area [cm^2]
ρ	Density [kg/m^3]
T_{in}	CO_2 temperature at compressor [K]
η_{is}	isentropic efficiency of compressor inlet [K]
η_p	Efficiency of pump [-]
CF	Capacity factor

REFERENCES

[1] Wang X. and Gu Y., "Oil Recovery and Permeability Reduction of a Tight Sandstone Reservoir in Immiscible and Miscible CO_2 Flooding Processes," *Industrial and Engineering Chemistry Research*, **2011**, *50*(4), 2388-2399.

[2] Dong M., Huang S. S., and Srivastava R., "Laboratory Study on Near-miscible CO_2 Injection in Steelman Reservoir," *Journal of Canadian Petroleum Technology*, **2001**, *40*(2), 53-61.

[3] Al-Wahaibi, Y. M. and A. K. Al-Hadrami, "The Influence of High Permeability Lenses on Immiscible, First- and Multi-contact Miscible Gas Injection," *Journal of Petroleum Science and Engineering 77*, **2011**, *77*, 313-325.

[4] Al-Wahaibi Y. M., Grattoni C. A., and Muggeridge A. H., "Drainage and Imbibition Relative Permeabilities at Near Miscible Conditions," *Journal of Petroleum Science and Engineering*, **2006**, *53*, 239-253.

[5] Parvazdavani M., Masihi M. and Ghazanfari M. H., "Gas-Oil Relative Permeability at near Miscible Condition: An Experimental and Modeling Approach," *Journal of Scientia Iranica*, **2012**, *20*, 626-636.

[6] Hussain F., Cinarand F., and Bedrikrikovetsky P., "Comparison of Methods for Drainage Relative Permeability Estimation from Displacement Tests," *SPE 129678*, Tulsa, Oklahoma, USA, **2010**.

[7] Trivedi J. J. and Babadagli T., "Experimental Investigations on the Flow Dynamics and Abandonment Pressure for CO_2 Sequestration and Oil Recovery in Artificially Fractured Cores," *Journal of Canadian Petroleum Technology*, **2010**, *49*(3), 22-27.

[8] McCain J. R. and William D., "*Properties of Petroleum Fluids*," Penn Well publishing Book Co, ISBN 0-87814-335-1, Tulsa, Oklahama, **1990**.

[9] Bui L. H., Tsau, J. S., and Willhite G. P., "Laboratory Investigations of CO_2 Near-Miscible Application in Arbuckle Reservoir," *SPE 129710*, Tulsa, Oklahoma, USA, **2010**.

[10] Sohrabi M., Danesh A., Tehrani D. H., and Jamiolahmady M., "Microscopic Mechanisms of Oil Recovery by Near-Miscible Gas Injection," *Transp Porous Med.*, **2008**, *72*, 351–367.

[11] Johnson E. F., Bossler D. P., and Naumann V. O., "Calculation of Relative Permeability from Displacement Experiments," *Trans. AIME*, **1959**, *216*, 370-372.

[12] Fletcher R., "Conjugate Direction Methods," Chapter 5 in Numerical Methods for Unconstrained Optimization, edited by W. Murray, Academic Press, New York, **1972**.

[13] Mohitpour M., Golshan H., and Murray A., "Pipeline Design & Construction: A Practical approach," *The American Society of Mechanical Engineers*, New York, **2000**.

[14] IEA Greenhouse Gas R&D Programme, Transmission of CO_2 and Energy, Report No. PH4/6, **2002**.

[15] Kreutz T., Williams R., Consonni S., and Chiesa P., "Co-production of Hydrogen, Electricity and CO_2 from Coal with Commercially Ready Technology Part B: Economic Analysis," *International Journal of Hydrogen Energy*, **2005**, *30*, 769-784.

[16] Asghari K. and Torabi F., "Laboratory Experimental Results of Huff 'n' Puff CO_2 Flooding in a Fractured Core System," Proceeding of the *SPE Annual Technical Conference and Exhibition* held in Anaheim California, US, **2007**.